Amplitude and Phase Synthesis at Cylindrical Apertures of Omnidirectional Dual-Reflector Antennas for Uniform Coverage

Pedro A. B. Leão, Tcharles V. B. Faria, and Fernando J. S. Moreira, *Senior Member, IEEE*

***Abstract*—This work presents a simple formulation to synthesize amplitude and phase distributions at cylindrical apertures of omnidirectional dual-reflector antennas. Adopting a tapered amplitude, the phase is obtained to provide an omnidirectional cosecant-squared radiation pattern with low sidelobe levels. Initially, the synthesis formulation is validated by the aperture method. Then, two distinct omnidirectional dual-reflector configurations are shaped and their radiation patterns are simulated by full-wave method-of-moments analyses and by ANSYS HFSS, to illustrate the usefulness of the synthesis technique.**

***Index Terms*—Cosecant-squared radiation pattern, omnidirectional dual-reflector antennas, reflector shaping.**

I. Introduction

DUAL-REFLECTOR antennas have been investigated in the past decades to provide omnidirectional radiation patterns with broader bandwidths and higher radiation efficiencies at millimetric wavelengths [1], [2], [3]. They complement a set of alternative geometries based on single reflectors [4], reflectarrays [5], and phased arrays [6], which provide shaped beams but over a coverage sector, and linear arrays [7], which inherently have narrow bandwidth. Many works have dealt with the reflector shaping of these antennas based on geometrical optics (GO). In some of them, both sub- and main-reflectors were shaped to establish a desired field amplitude at the cylindrical aperture of the main reflector, but imposing a uniform phase for broadside radiation patterns [1], [2], [3]. Such works presented relatively compact dual-reflector geometries. In other works, only the main reflector was shaped, generally to provide a cosecant-squared radiation pattern in the elevation plane for uniform coverage in local multipoint distribution systems, but with the expense of more elongated main reflectors [8], [9].

In this work, the objective is to present a simple formulation that establishes a nonuniform phase distribution at a cylindrical aperture for a given amplitude distribution (which can by properly tapered to reduce undesirable sidelobe levels) and a desired omnidirectional radiation pattern in the antenna elevation plane. After the amplitude and phase of the aperture field are defined, both sub- and main-reflectors can be shaped using well established GO techniques [10], [11], [12]. As will be demonstrated, more compact dual-reflector geometries than those investigated in [8] and [9] can be attained.

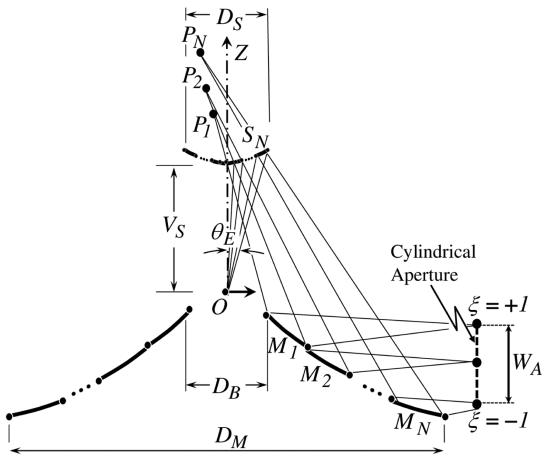

Fig. 1. OADC-like configuration with reflector generatrices represented by local conic sections.

The rest of this letter is organized as follows. In Section II, the formulation which defines the aperture phase distribution is presented. It is based on the theory developed in [13] for determining the phase distribution over a planar aperture, but extended here for a cylindrical aperture. The formulation is further suited for a tapered amplitude at the cylindrical aperture, to reduce sidelobe levels and ripples in the desired omnidirectional cosecant-squared radiation pattern. In Section III, the aperture method (Ap-M) is employed to investigate the formulation of Section II. Results are compared with those obtained for a uniform aperture amplitude to demonstrate the reduction of the sidelobe levels attained by the proposed tapered amplitude. In Section IV, two antenna configurations are shaped to provide the desired GO field at the cylindrical aperture: one based on an omnidirectional axis-displaced Cassegrain (OADC), as illustrated in Fig. 1, and another on an omnidirectional axis-displaced Ellipse (OADE), illustrated in Fig. 2. Full-wave analyses based on the method of moments (MoM) and software ANSYS HFSS are presented

Manuscript received 12 April 2024; accepted 15 May 2024. Date of publication 22 May 2024; date of current version 6 September 2024. This work was supported in part by CNPq under Grant 303257/2022-9; in part by FAPEMIG under Grant PPM-00384-18; and in part by CAPES-PROEX, Brazil. *(Corresponding author: Pedro A. B. Leão.)*

Pedro A. B. Leão and Tcharles V. B. Faria are with the Graduate Program in Electrical Engineering, Universidade Federal de Minas Gerais (UFMG), Belo Horizonte 31270-901, Brazil (e-mail: pedrobessaleao@gmail.com).

Fernando J. S. Moreira is with the Graduate Program in Electrical Engineering, Universidade Federal de Minas Gerais (UFMG), Belo Horizonte 31270-901, Brazil, and also with the Electronics Engineering Department, UFMG, Belo Horizonte 31270-901, Brazil (e-mail: fernandomoreira@ufmg.br).

Digital Object Identifier 10.1109/LAWP.2024.3404370

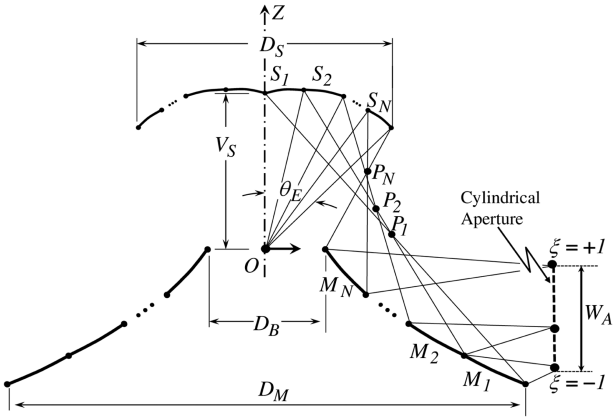

Fig. 2. OADE-like configuration with reflector generatrices represented by local conic sections.

to illustrate the usefulness of the synthesis technique. Finally, Section V concludes this letter.

II. Nonuniform Phase Synthesis Technique

The determination of the nonuniform phase distribution $\psi(\xi)$ over the cylindrical aperture is based on [13]. There, the authors employed the stationary phase method to establish a differential equation for $\psi(\xi)$ over a planar aperture as function of the far-field observation direction. The equation can be easily adapted to the present cylindrical geometry

$$\frac{d\psi}{d\xi} = -k\,\frac{W_A}{2}\,u(\xi) \tag{1}$$

where $k = 2\pi/\lambda$, W_A is the height of the cylindrical aperture, and ξ is the normalized aperture coordinate along the axial direction, such that $\xi = -1$ at the bottom of the aperture and $\xi = 1$ at the top (see Figs. 1 and 2). Finally, $u = \sin(\theta - 3\pi/2)$, where θ is the angle of the far-field direction, with $\theta = \pi/2$ (i.e., $u = 0$) being normal to the cylindrical aperture. The mapping function $u(\xi)$ relates an aperture point to a corresponding far-field direction and is obtained by the conservation of energy as follows.

A normalized aperture power density $g(\xi)$ is defined as

$$g(\xi) = \frac{\int_{-1}^{\xi} G_A(\eta)\,d\eta}{\int_{-1}^{1} G_A(\eta)\,d\eta} \tag{2}$$

where G_A is a prescribed power density at the aperture and η is a dummy integration variable. Furthermore, at the far field the following normalized radiated power density is defined:

$$h(u) = \frac{\int_{-1}^{u} G_F(\tau)\,d\tau}{\int_{-1}^{1} G_F(\tau)\,d\tau} \tag{3}$$

where G_F represents the desired radiation pattern in the elevation plane and τ is a dummy integration variable. The mapping function $u(\xi)$ is then obtained by imposing the conservation of energy

$$h(u) = g(\xi). \tag{4}$$

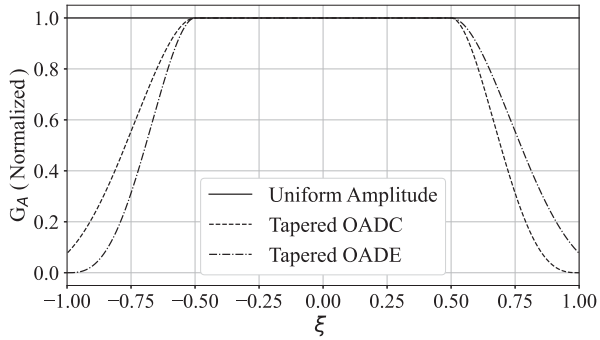

Fig. 3. G_A distributions. The tapered ones have $\alpha_1 = \alpha_2 = 3, \beta_1 = \beta_2 = 1$, $\xi_1 = -0.5$, and $\xi_2 = 0.5$. For an OADC, $\chi_1 = 0.29$ and $\chi_2 = 0$; for an OADE, $\chi_1 = 0$ and $\chi_2 = 0.29$.

Depending on the complexity of G_A and G_F, (1) and (4) may have to be numerically determined to obtain the aperture field as function of $\sqrt{G_A}$ (amplitude) and ψ (phase).

Now we proceed to develop particular equations for G_A and G_F. In [13], $G_A = 1$ is adopted (for a planar aperture), which provides, from (2), $g(\xi) = (\xi - 1)/2$. However, such uniform amplitude may provide larger sidelobe levels. To reduce these undesired sidelobe levels, we propose the distribution adopted in [3], which proved to be very effective

$$G_A(\xi) = \begin{cases} (\Delta_1)^{\alpha_1}\left[1 + (\alpha_1/\beta_1)(1-\Delta_1)\right]^{\beta_1}, & -1 \le \xi \le \xi_1 \\ 1, & \xi_1 < \xi < \xi_2 \\ (\Delta_2)^{\alpha_2}\left[1 + (\alpha_2/\beta_2)(1-\Delta_2)\right]^{\beta_2}, & \xi_2 \le \xi \le 1 \end{cases} \tag{5}$$

where

$$\Delta_1 = \chi_1 + (1-\chi_1)(1+\xi)/(1+\xi_1) \tag{6}$$

$$\Delta_2 = \chi_2 + (1-\chi_2)(1-\xi)/(1-\xi_2) \tag{7}$$

with α_i, β_i, ξ_i, and χ_i $(i = 1, 2)$ controlling the tapered distribution at the cylindrical aperture edges. The distribution (5) is continuous and has continuous first derivative, necessary for an efficient GO reflector shaping. For an OADC-like configuration (see Fig. 1) $\chi_2 = 0$ to obtain $G_A(1) = 0$, while for an OADE (see Fig. 2) $\chi_1 = 0$ for $G_A(-1) = 0$, as explained in [3]. Fig. 3 illustrates different $G_A(\xi)$ distributions.

For a cosecant-squared radiation pattern one should define

$$G_F(u) = \begin{cases} 0, & -1 \le u \le u_1 \\ (A/u)^2, & u_1 < u < u_2 \\ 0, & u_2 \le u \le 1 \end{cases} \tag{8}$$

where A is a normalization constant, and $u_1 = \sin(\theta_1 - 3\pi/2)$ and $u_2 = \sin(\theta_2 - 3\pi/2)$ define the starting and ending directions of the cosecant-squared pattern. Substituting (8) into (3), the following analytical solution is obtained:

$$h(u) = \frac{u_2\,(u - u_1)}{u\,(u_2 - u_1)}. \tag{9}$$

III. Validation of the Proposed Technique

Due to the intricacy of the tapered G_A distribution (5), (2) and, consequently, (1) and (4) must be numerically solved. So, before shaping the antenna reflectors, a simple analysis based on

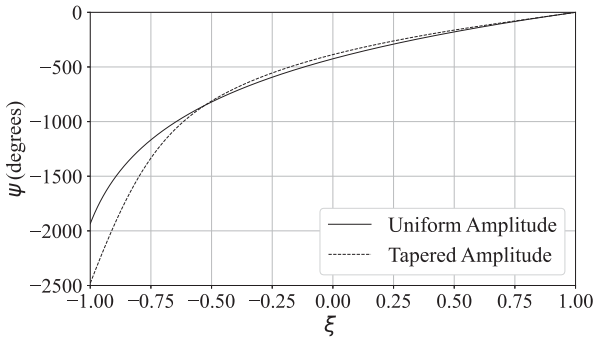

Fig. 4. ψ distributions for the uniform and tapered amplitudes.

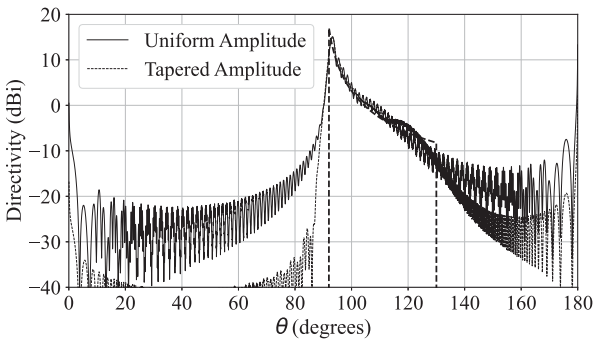

Fig. 5. Ap-M radiation patterns for the uniform and tapered G_A distributions.

the Ap-M is conducted to verify the formulation and to establish if (5) can indeed reduce undesirable sidelobe levels. For $W_A = 50\lambda$, $\theta_1 = 92^\circ$, and $\theta_2 = 130^\circ$, phase $\psi(\xi)$ was determined for a uniform amplitude distribution ($G_A = 1$) and for (5) with the OADE parameters (i.e., $\chi_1 = 0$ and $\chi_2 = 0.29$) declared in the caption of Fig. 3.

Fig. 4 shows the two $\psi(\xi)$ distributions obtained from the numerical evaluation of (1) and (4). From the figure one observes that the phase variation is more intense at the bottom of the cylindrical aperture ($\xi < 0$) in order to provide the necessary roll-off of the cosecant-squared pattern.

Fig. 5 presents the cosecant-squared pattern of (8) and the Ap-M radiation patterns obtained for the uniform (solid line) and tapered (dashed) amplitude distributions. Ap-M was employed with the amplitude and phase of the aperture equivalent sources given by $\sqrt{G_A}$ and ψ, respectively. Due to the uniformity of (5) at $\xi_1 < \xi < \xi_2$, the tapered distribution is capable of reducing sidelobe levels and undesirable ripples at $\theta_1 < \theta < \theta_2$ without severely compromising directivity (the maximum directivities at $\theta \approx 93^\circ$ are 15.09 and 14.87 dBi for the uniform and tapered amplitudes, respectively).

IV. Case Studies

The asymptotic technique of Section II and the Ap-M adopted in Section III to simulate the radiation patterns do not take into account diffraction effects at reflector edges nor mutual coupling among reflectors and feed horn. So, in this section the formulation of Section II is employed to shape two distinct omnidirectional dual-reflector configurations: an OADC (see Fig. 1) and an OADE (see Fig. 2). To show the usefulness of the present formulation, the shaped reflector antennas are then analyzed by the MoM and by ANSYS HFSS software. The feed horn (coaxial horn excited by the fundamental TEM mode [3]) is included in the analyses. The MoM algorithm has been successfully used in many other works (e.g., [3], [9], and [12]).

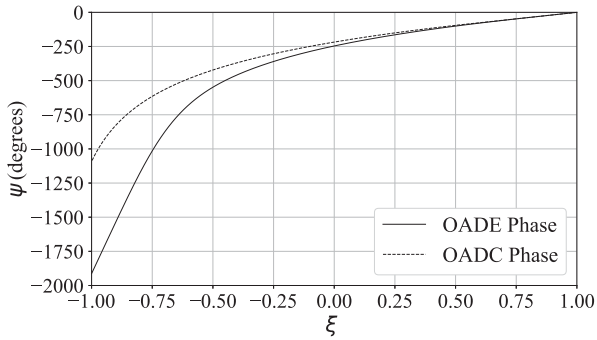

Fig. 6. ψ distributions for shaped OADC and OADE.

For the GO shaping of both reflectors, the technique in [12] was employed. It uses local conic sections to describe the generatrices of the circularly symmetric reflectors (see Figs. 1 and 2). The technique permits the control of the amplitude and phase of the aperture field without the need of solving any ordinary differential equation [12]. The feed horn radiated power density, necessary for the GO shaping, was represented by the model described in [3, eq. (14)]. The aperture field amplitude ($\sqrt{G_A}$) and phase (ψ) were obtained from the formulation of Section II, with G_A given by (5) and aiming a cosecant-squared pattern (8) with $\theta_1 = 92^\circ$ and $\theta_2 = 135^\circ$. The shaping initial geometric parameters (i.e., reflector diameters, subreflector edge angle, etc.) were obtained from the classical (nonshaped) configurations investigated in [14]. No attempts were made to optimize the designs.

Starting with an OADC, its initial geometric parameters (see Fig. 1) were obtained with $D_M = 69\lambda$, $D_B = 6\lambda$, $V_S = 31.5\lambda$, $D_S = 69\lambda$, and $\theta_E = 56.2^\circ$, corresponding to $W_A = 30\lambda$ [14]. For the tapered amplitude, G_A was calculated from (5) with $\alpha_1 = \alpha_2 = 9$, $\beta_1 = \beta_2 = 3$, $\xi_1 = -0.5$, $\xi_2 = 0.5$, $\chi_1 = 0.87$, and $\chi_2 = 0$. The numerical solution of (1) and (4) provided the phase distribution ψ illustrated with dashed line in Fig. 6 and basically has the same behavior of the phases in Fig. 4. With G_A, ψ, and the initial geometric parameter, the GO reflector shaping provided the generatrices shown in Fig. 7(a) together with the initial classical (nonshaped) geometry in dashed lines. One observes from this figure that the shaped main reflector is not elongated as those shaped in [8] and [9], as desired.

The MoM and ANSYS HFSS radiation patterns at 30 GHz are shown in Fig. 8 with the corresponding Ap-M pattern and a 3-D sector-cut view of the antenna. The coaxial horn used in [3] was included in both analyses. The MoM simulation included the mutual coupling among the two reflectors and horn. The ANSYS HFSS simulation analyzed the feed horn with finite elements and the reflectors' radiation with physical optics. From Fig. 8 one observes that the synthesis provided a radiation pattern with the desired profile, with ripples accentuated by diffraction effects. At $45^\circ < \theta < 65^\circ$ the feed spillover is apparent. For $\theta > 160^\circ$ one

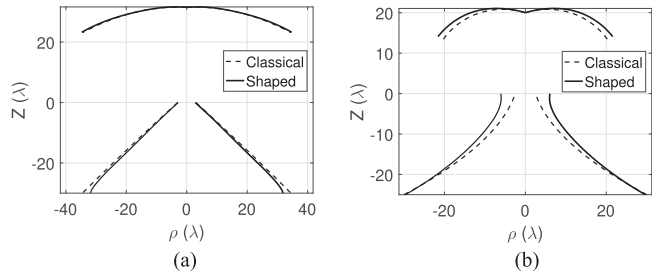

Fig. 7. Generatrices of the classical (dashed lines) and shaped (solid lines) (a) OADC and (b) OADE reflectors.

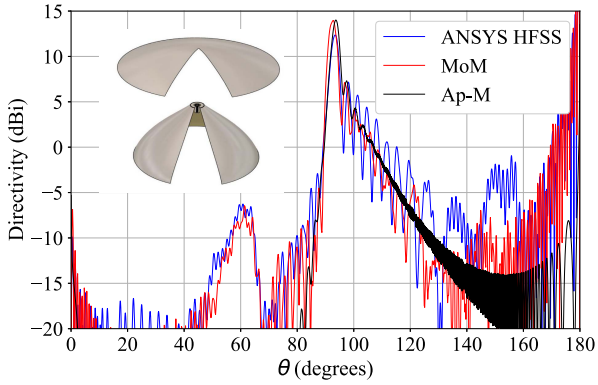

Fig. 8. Radiation patterns of the shaped OADC antenna.

TABLE I
MAXIMUM DIRECTIVITIES D_o (WITH RESPECTIVE DIRECTIONS θ), HPBW, AND RMS ERRORS (FOR $\theta_1 \leq \theta \leq \theta_2$) AT 30 GHZ

Model	Method	D_o (dBi)	θ	HPBW	RMSE (dB)
OADC	HFSS	12.36	93.45°	3.05°	4.11
	MoM	13.96	92.70°	3.23°	3.30
	Ap-M	14.01	93.67°	2.89°	1.92
OADE	HFSS	13.94	92.90°	2.90°	3.52
	MoM	14.96	92.88°	2.70°	3.53
	Ap-M	13.53	93.67°	3.41°	1.62

observes the increase in sidelobe levels due to the diffraction at the main-reflector edge. The maximum directivities, half-power beamwidth (HPBW), and rms errors of the patterns' ripples with respect to the cosecant-squared profile for $\theta_1 \leq \theta \leq \theta_2$ are listed in Table I.

In the second case, an OADE (see Fig. 2) was shaped with initial parameters $D_M = 60\lambda$, $D_B = 5\lambda$, $V_S = 20\lambda$, $z_B = 0$, $D_S = 40.7\lambda$, and $\theta_E = 56.2°$, providing $W_A = 25\lambda$ (about 5λ smaller than the previous OADC). The tapered amplitude was calculated from (5) with $\alpha_1 = \alpha_2 = 3$, $\beta_1 = \beta_2 = 1$, $\xi_1 = -0.5$, $\xi_2 = 0.5$, $\chi_1 = 0$, and $\chi_2 = 0.29$. The phase ψ is illustrated with solid line in Fig. 6. The GO shaping provided the generatrices shown in Fig. 7(b) with the initial classical geometry in dashed lines. Once more, the simultaneous shaping of both reflectors provided a main reflector that is not elongated as in [8] and [9].

The OADE radiation patterns at 30 GHz are shown in Fig. 9 with a 3-D sector-cut view of the antenna. One observes that

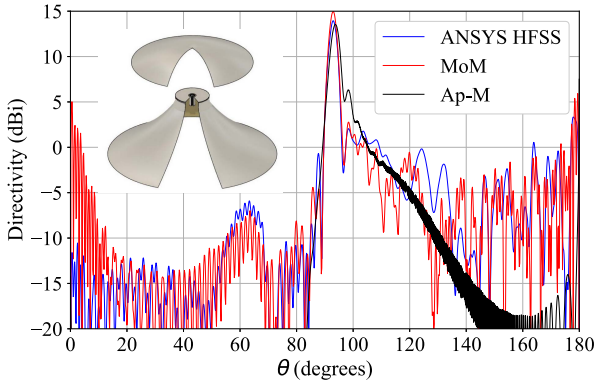

Fig. 9. Radiation patterns of the shaped OADE antenna.

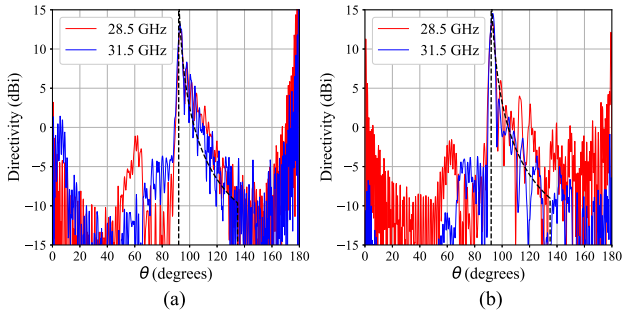

Fig. 10. MoM radiation patterns at 28.5 GHz and 31.5 GHz: (a) OADC and (b) OADE.

the synthesis provided a radiation pattern essentially with the cosecant-squared profile, with ripples accentuated by diffraction effects. Once more, the feed spillover is apparent. The sidelobe levels for $\theta > 160°$ are less accentuated than in Fig. 8 due to the inversion of the feed illumination provided by the OADE [14]. Maximum directivities, HPBW, and rms errors of the patterns' ripples with respect to the cosecant-squared profile for $\theta_1 \leq \theta \leq \theta_2$ are given in Table I.

To show the stability of the shaping procedure, MoM analyses were repeated at 28.5 GHz and 31.5 GHz. Fig. 10 shows that the desired cosecant-squared pattern is still attained for both configurations, with small loss of directivity and small increase of feed spillover, as the feed was not designed for broadband performance [3]. The largest RMSE for $\theta_1 \leq \theta \leq \theta_2$ is 4.95 dB for the OADE at 28.5 GHz.

V. CONCLUSION

A technique for defining the GO field over the cylindrical aperture of omnidirectional dual-reflector antennas was proposed, incorporating a tapered amplitude distribution to reduce sidelobe levels. The adopted tapered amplitude and the necessary formulation for the phase synthesis were initially validated by the Ap-M, and the reduction of the radiation pattern sidelobe levels was confirmed. Then, two dual-reflector antennas (an OADC and an OADE) were shaped to attain synthesized aperture distributions, and further analyzed by the MoM and ANSYS HFSS software to confirm the efficiency and usefulness of the aperture synthesis presented in Section II for realistic antenna designs.

REFERENCES

[1] R. A. Penchel, S. R. Zang, J. R. Bergmann, and F. J. S. Moreira, "Design of wideband omnidirectional dual-reflector antennas in mm-waves," *IEEE Antennas Wireless Propag. Lett.*, vol. 18, no. 5, pp. 906–910, May 2019.

[2] A. G. Pino, A. M. A. Acuña, and J. O. R. Lopez, "An omnidirectional dual-shaped reflector antenna," *Microw. Opt. Technol. Lett.*, vol. 27, no. 5, pp. 371–374, Dec. 2000.

[3] F. J. S. Moreira, A. Prata Jr., and J. R. Bergmann, "GO shaping of omnidirectional dual-reflector antennas for a prescribed equi-phase aperture field distribution," *IEEE Trans. Antennas Propag.*, vol. 55, no. 1, pp. 99–106, Jan. 2007.

[4] H. Ahmadabadi, S. Mallahzadeh, and A. Torabi, "Wide beam reflector antenna with cosecant-squared pattern," *Int. J. Electron. Commun.*, vol. 116, Mar. 2020, Art. no. 153064.

[5] K. Q. Henderson and N. Ghalichechian, "Triangular and rectangular lattices for cosecant-squared-shaped beam reflectarrays," *IEEE Antennas Wireless Propag. Lett.*, vol. 20, no. 10, pp. 2058–2062, Oct. 2021.

[6] J. Puskely, T. Mikulasek, Y. Aslan, A. Roederer, and A. Yarovoy, "5G SIW-based phased antenna array with cosecant-squared shaped pattern," *IEEE Trans. Antennas Propag.*, vol. 70, no. 1, pp. 250–259, Jan. 2022.

[7] C. Zhao, Y. Aslan, A. Yarovoy, and A. Roederer, "Cosecant-squared shaped pattern stability with frequency in series-fed antennas at mm-waves," in *Proc. IEEE Conf. Antenna Meas. Appl.*, 2023, pp. 555–559, doi: 10.1109/CAMA57522.2023.10352663.

[8] R. Vallauri, P. Besso, A. Avitabile, R. Bills, and R. Brachat, "Azimuthally omnidirectional antenna with vertical or horizontal polarisation for LMDS in the 40 GHz band," in *Proc. Millennium Conf. Antennas Propag.*, 2000, Art. no. 555.

[9] R. A. Penchel, J. R. Bergmann, and F. J. S. Moreira, "Main-reflector shaping of omnidirectional dual reflectors using local conic sections," *IEEE Trans. Antennas Propag.*, vol. 61, no. 8, pp. 4379–4383, Aug. 2013.

[10] V. Galindo, "Design of dual-reflector antennas with arbitrary phase and amplitude distributions," *IEEE Trans. Antennas Propag.*, vol. AP-12, no. 4, pp. 403–408, Jul. 1964.

[11] J. J. Lee, L. I. Parad, and R. S. Chu, "A shaped offset-fed dual-reflector antenna," *IEEE Trans. Antennas Propag.*, vol. AP-27, no. 2, pp. 165–171, Mar. 1979.

[12] T. V. B. Faria and F. J. S. Moreira, "New technique for shaping axisymmetric dual-reflector antennas using conic sections to control aperture illumination," *IET Microw. Antennas Propag.*, vol. 14, no. 12, pp. 1310–1315, 2020.

[13] A. K. Chakraborty, B. N. Das, and G. S. Sanyal, "Determination of phase functions for a desired one-dimensional pattern," *IEEE Trans. Antennas Propag.*, vol. AP-29, No 3, pp. 502–506, May 1981.

[14] F. J. S. Moreira and J. R. Bergmann, "Classical axis-displaced dual-reflector antennas for omnidirectional coverage," *IEEE Trans. Antennas Propag.*, vol. 53, no. 9, pp. 2799–2808, Sep. 2005.